COMPUTER GRAPHICS AND IMAGE PROCESSING 18, 236–258 (1982)

Elliptic Fourier Features of a Closed Contour[1]

FRANK P. KUHL

U.S. Army Armament Research and Development Command, Dover, New Jersey 07801

AND

CHARLES R. GIARDINA

Fairleigh Dickinson University, Teaneck, New Jersey 07070

Received June 22, 1981

A direct procedure for obtaining the Fourier coefficients of a chain-encoded contour is presented. Advantages of the procedure are that it does not require integration or the use of fast Fourier transform techniques, and that bounds on the accuracy of the image contour reconstruction are easy to specify. Elliptic properties of the Fourier coefficients are shown and used for a convenient and intuitively pleasing procedure of normalizing a Fourier contour representation. Extension of the contour representation to arbitrary objects at arbitrary aspect angle is discussed. The procedures have direct application to a variety of pattern recognition problems that involve analysis of well-defined image contours.

1. INTRODUCTION

Fourier descriptors have been successfully used by many investigators [1–4] for the characterization of closed contours. In this paper, a particularly simple way of obtaining the Fourier coefficients of a chain-encoded [5, 12] contour is presented as well as bounds on the error of such a representation and, also, an intuitively pleasing way of normalizing the Fourier coefficients using a harmonic, elliptic description of the contour [6, 7]. The resulting Fourier descriptors are invariant with rotation, dilation and translation of the contour, and also with the starting point on the contour, but lose no information about the shape of the contour.

2. FOURIER COEFFICIENTS OF A CHAIN CODE

The chain code first described by Freeman [5] approximates a continuous contour by a sequence of piecewise linear fits that consist of eight standardized line segments. The code of a contour is then the chain V of length K

$$V = a_1 a_2 a_3 \ldots a_K,$$

where each link a_i is an integer between 0 and 7 oriented in the direction $(\pi/4)a_i$ (as measured counter-clockwise from the X axis of an X–Y coordinate system) and of length 1 or $\sqrt{2}$ depending, respectively, on whether a_i is even or odd. The vector

[1]The views, opinions, and/or findings contained in this paper are those of the authors and should not be construed as an official Department of the Army position, policy or decision.

The citation in this paper of the names of commercial firms or commercially available products or services does not constitute official endorsement or approval of such commercial firms, products, or services by the United States Government.

0146-664X/82/030236-23$02.00/0
Copyright © 1982 by Academic Press, Inc.

representation of the link a_i, using phasor notation, is

$$\left(1 + \frac{(\sqrt{2}-1)}{2}(1-(-1)^{a_i})\right) \angle \frac{\pi}{4} a_i.$$

An example of a chain code,

$$V_1 = 0005676644422123,$$

is shown in Fig. 1b, using the method of deriving a chain code from an area-quantized image (Fig. 1a) described by Kuhl [8]. The Fourier coefficients of a chain encoded

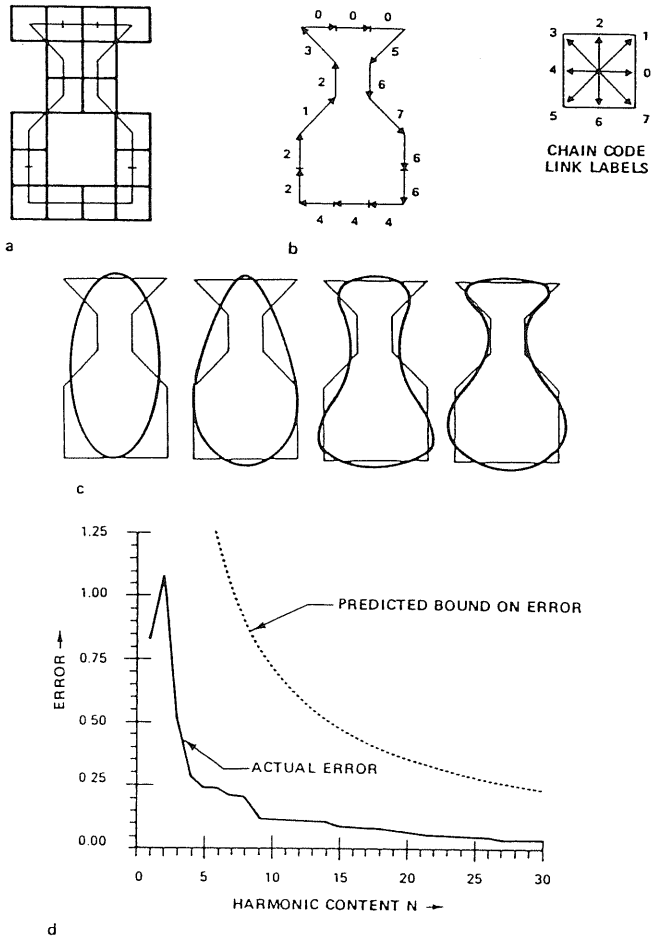

FIG. 1. Properties of the chain code V_1 = 0005676644422123. (a) Area-quantized image. (b) Chain code of image. (c) 1-, 2-, 3-, and 4-harmonic representations of the chain code V_1. (d) Actual error and predicted bound on error versus harmonic content.

contou developed in this section of the paper for a particular starting point on the contour. The Fourier series representation is appropriate for the chain code because the code repeats on successive traversals of the contour.

Elementary properties of the chain code are easily described. Assuming that the chain code is followed at constant speed, the time needed to traverse a particular link a_i is

$$\Delta t_i = 1 + \left(\frac{\sqrt{2}-1}{2}\right)(1-(-1)^{a_i}).$$

The time required to traverse the first p links in the chain is

$$t_p = \sum_{i=1}^{p} \Delta t_i$$

and the basic period of the chain code is $T = t_K$. The changes in the x, y projections of the chain as the link a_i is traversed are

$$\Delta x_i = \operatorname{sgn}(6-a_i)\operatorname{sgn}(2-a_i),$$
$$\Delta y_i = \operatorname{sgn}(4-a_i)\operatorname{sgn}(a_i),$$

where

$$\operatorname{sgn}(Z)\begin{cases} 1 & Z>0 \\ 0 & Z=0 \\ -1 & Z<0, \end{cases}$$

and, arbitrarily locating the starting point of the chain code at the origin, the projections on x and y of the first p links of the chain are, respectively,

$$x_p = \sum_{i=1}^{p} \Delta x_i,$$
$$y_p = \sum_{i=1}^{p} \Delta y_i.$$

The Fourier series expansion for the x projection of the chain code of the complete contour is defined as

$$x(t) = A_0 + \sum_{n=1}^{\infty} a_n \cos\frac{2n\pi t}{T} + b_n \sin\frac{2n\pi t}{T},$$

where

$$A_0 = \frac{1}{T}\int_0^T x(t)\,dt,$$
$$a_n = \frac{2}{T}\int_0^T x(t)\cos\frac{2n\pi t}{T}\,dt,$$
$$b_n = \frac{2}{T}\int_0^T x(t)\sin\frac{2n\pi t}{T}\,dt.$$

The Fourier coefficients corresponding to the nth harmonic a_n and $(B_0 \equiv 0)$ are most easily found because $x(t)$ is piecewise linear and continuous for all time. The derivation of the coefficients here involves the time derivative $\dot{x}(t)$, which consists of the sequence of piecewise constant derivatives $\Delta x_p/\Delta t_p$ associated with the time intervals $t_{p-1} < t < t_p$ for values of p in the range of $1 \le p \le K$. The time derivative is periodic with period T and can itself be represented by the Fourier series

$$\dot{x}(t) = \sum_{n=1}^{\infty} \alpha_n \cos\frac{2n\pi t}{T} + \beta_n \sin\frac{2n\pi t}{T},$$

where

$$\alpha_n = \frac{2}{T}\int_0^T \dot{x}(t)\cos\frac{2n\pi t}{T}\,dt,$$
$$\beta_n = \frac{2}{T}\int_0^T \dot{x}(t)\sin\frac{2n\pi t}{T}\,dt.$$

Then

$$\alpha_n = \frac{2}{T}\sum_{p=1}^{K}\frac{\Delta x_p}{\Delta t_p}\int_{t_{p-1}}^{t_p}\cos\frac{2n\pi t}{T}\,dt$$
$$= \frac{2}{T}\sum_{p=1}^{K}\frac{\Delta x_p}{\Delta t_p}\left(\sin\frac{2n\pi t_p}{T} - \sin\frac{2n\pi t_{p-1}}{T}\right)$$

and

$$\beta_n = \frac{2}{T}\sum_{p=1}^{K}\frac{\Delta x_p}{\Delta t_p}\int_{t_{p-1}}^{t_p}\sin\frac{2n\pi t}{T}\,dt$$
$$= -\frac{2}{T}\sum_{p=1}^{K}\frac{\Delta x_p}{\Delta t_p}\left(\cos\frac{2n\pi t_p}{T} - \cos\frac{2n\pi t_{p-1}}{T}\right).$$

But $\dot{x}(t)$ is also obtained directly from its definition as

$$\dot{x}(t) = \sum_{n=1}^{\infty} -\frac{2n\pi}{T}a_n \sin\frac{2n\pi t}{T} + \frac{2n\pi}{T}b_n \cos\frac{2n\pi t}{T}.$$

Equating coefficients from the two expressions of $\dot{x}(t)$,

$$a_n = \frac{T}{2n^2\pi^2}\sum_{p=1}^{K}\frac{\Delta x_p}{\Delta t_p}\left[\cos\frac{2n\pi t_p}{T} - \cos\frac{2n\pi t_{p-1}}{T}\right],$$
$$b_n = \frac{T}{2n^2\pi^2}\sum_{p=1}^{K}\frac{\Delta x_p}{\Delta t_p}\left[\sin\frac{2n\pi t_p}{T} - \sin\frac{2n\pi t_{p-1}}{T}\right].$$

The Fourier series expansion for the y projection of the chain code of the complete

contour is similarly found as follows:

$$y(t) = C_0 + \sum_{n=1}^{\infty} c_n \cos\frac{2n\pi t}{T} + d_n \sin\frac{2n\pi t}{T},$$

where

$$c_n = \frac{T}{2n^2\pi^2}\sum_{p=1}^{K}\frac{\Delta y_p}{\Delta t_p}\left[\cos\frac{2n\pi t_p}{T} - \cos\frac{2n\pi t_{p-1}}{T}\right],$$

$$d_n = \frac{T}{2n^2\pi^2}\sum_{p=1}^{K}\frac{\Delta y_p}{\Delta t_p}\left[\sin\frac{2n\pi t_p}{T} - \sin\frac{2n\pi t_{p-1}}{T}\right].$$

The applicability of the expressions for the Fourier coefficients extends to the generalized chain code described by Freeman [9] as well as to any piecewise linear representation of a contour since no constraints are made on the incremental changes Δx_p and Δy_p ($\Delta t_p = (\Delta x_p^2 + \Delta y_p^2)^{1/2}$).

The DC components in these Fourier series are as follows:

$$A_0 = \frac{1}{T}\sum_{p=1}^{K}\left[\frac{\Delta x_p}{2\,\Delta t_p}\left(t_p^2 - t_{p-1}^2\right) + \xi_p\left(t_p - t_{p-1}\right)\right]$$

$$C_0 = \frac{1}{T}\sum_{p=1}^{K}\frac{\Delta y_p}{2\,\Delta t_p}\left(t_p^2 - t_{p-1}^2\right) + \delta_p\left(t_p - t_{p-1}\right),$$

where

$$\xi_p = \sum_{j=1}^{p-1}\Delta x_j - \frac{\Delta x_p}{\Delta t_p}\sum_{j=1}^{p-1}\Delta t_j,$$

$$\delta_p = \sum_{j=1}^{p-1}\Delta y_j - \frac{\Delta y_p}{\Delta t_p}\sum_{j=1}^{p-1}\Delta t_j,$$

and

$$\xi_1 = \delta_1 = 0.$$

Graphic examples of 1-, 2-, 3-, and 4-harmonic Fourier approximations of the chain code V_1 are shown in Fig. 1c.

3. NUMBER OF HARMONICS NEEDED IN THE FOURIER APPROXIMATION

It is useful to be able to specify the number of harmonics required such that a truncated Fourier approximation to a contour be in error by no more than ϵ in the x or y dimension. Let

$$X_N = A_0 + \sum_{n=1}^{N} a_n \cos\frac{2n\pi t}{T} + b_n \sin\frac{2n\pi t}{T},$$

$$Y_N = C_0 + \sum_{n=1}^{N} c_n \cos\frac{2n\pi t}{T} + d_n \sin\frac{2n\pi t}{T},$$

be the Fourier series truncated after N harmonics for the $x(t)$ and $y(t)$ projections, respectively, and define the error, ϵ, as

$$\epsilon = \max\left[\sup_t |x(t) - x_N(t)|, \sup_t |y(t) - y_N(t)|\right].$$

Then it is shown by Giardina and Kuhl [7] that ϵ is bounded by the expression

$$\epsilon \le \frac{T}{2\pi^2 N}\max\left[\bigvee_0^T(\dot{x}(t)), \bigvee_0^T(\dot{y}(t))\right],$$

where the total variation of the derivative $\dot{x}(t)$ has been symbolized as $V_0^T(\dot{x}(t))$ and of the derivative $\dot{y}(t)$ as $V_0^T(\dot{y}(t))$. The derivatives for the link a_i are

$$\dot{x}_i = \frac{\Delta x_i}{\Delta t_i},$$

$$\dot{y}_i = \frac{\Delta y_i}{\Delta t_i},$$

and can be tabulated according to the value of a_i as shown in Table 1. Then, the total variations of $\dot{x}(t)$ and $\dot{y}(t)$ are, respectively:

$$\bigvee_0^T(\dot{x}(t)) = \left(\sum_2^K \dot{x}_i - \dot{x}_{i-1}\right) + |\dot{x}_K - \dot{x}_1|,$$

$$\bigvee_0^T(\dot{y}(t)) = \left(\sum_2^K \dot{y}_i - \dot{y}_{i-1}\right) + |\dot{y}_K + \dot{y}_1|.$$

A graph of the actual error, ϵ, versus the number of harmonics, N, used in the Fourier approximation is shown in Fig. 1d for the chain code V_1. The predicted bounds on the error are shown superimposed on the graph as predicted by the maximum, total-variation formula.

The following five chain codes are now examined:

V_2 = 11172206667666444444222,

V_3 = 5412343001010007711075454506541344446,

V_4 = 00466026046246532671240224,

V_5 = 00310704547644571534504133142060O,

V_6 = 233344676654443326770001223254543322156677010144432211045566700032110773345567100077623344450077776.

They are examples of image contours of increasingly greater complexity (i.e., wiggliness) as shown in Figs. 2 through 6. In each figure the chain-code representation of the image contour is displayed with superimposed Fourier approximations, which incorporate increasingly higher harmonic content. Also, the actual error and *one-half* the predicted bound on the error versus harmonic content, N, are shown at

TABLE I

x and y Derivatives of Link a_i

a_i	$\dot{x}_i$	$\dot{y}_i$
0	1.0	0.0
1	0.707	0.707
2	0.0	1.0
3	−0.707	0.707
4	−1.0	0.0
5	−0.707	−0.707
6	0.0	−1.0
7	0.707	−0.707

the bottom of each figure. The factor of *one-half* has been incorporated on the predicted bound because it has been experimentally found that for all but the most simple figures, as for example an equilateral triangle, the bound is quite conservative. It is apparent from inspection of the figures that as the contour becomes more complex, the predicted bound becomes more conservative, and that to make comparisons of the accuracy of harmonic reconstruction for different contours both plots of ϵ must be normalized against $T = t_K$; i.e., use $\epsilon' = \epsilon/T$.

The predicted bound on ϵ offers the advantage of quick and easy computation compared to the calculation of the actual error, but a heuristic factor (e.g., division by a constant) must be applied to the bound to obtain a closer approximation to the error curve. The heuristic factor would be developed by experimentation for particular applications and might, for example, be a function of the number of large angular changes in the contour.

4. PROPERTIES OF THE FOURIER EXPANSION OF A CLOSED CONTOUR

The truncated Fourier approximation to a closed contour can be written as

$$x(t) = A_0 + \sum_{n=1}^{N} X_n,$$

$$y(t) = C_0 + \sum_{n=1}^{N} Y_n,$$

where the components of the projections X_n, Y_n $(1 \le n \le N)$ are

$$X_n(t) = a_n \cos\frac{2\pi nt}{T} + b_n \sin\frac{2\pi nt}{T},$$

$$Y_n(t) = c_n \cos\frac{2\pi nt}{T} + d_n \sin\frac{2\pi nt}{T}.$$

It has been shown by Kuhl [7] that the points (X_n, Y_n) all have elliptic loci, and that the Fourier approximation to the original contour can be viewed as the addition in proper phase relationship of rotating phasors, which are defined by the projections. Each rotating phasor has an elliptic locus and rotates faster than the first harmonic by its harmonic number n. This is demonstrated in Fig. 7 with considerable artistic

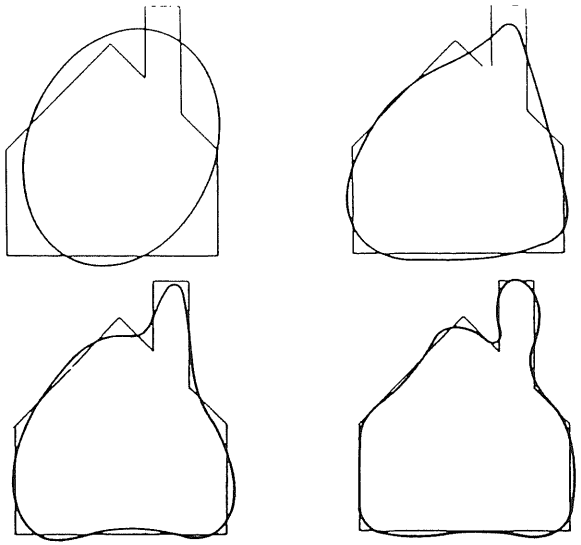

a

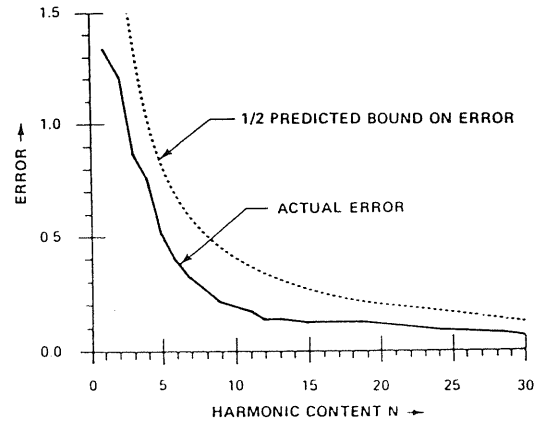

b

FIG. 2. Properties of the chain code V_2 = 11172206667666444444222. (a) 1-, 2-, 5-, and 7-harmonic representations of the chain code. (b) Actual error and predicted bound on error versus harmonic content.

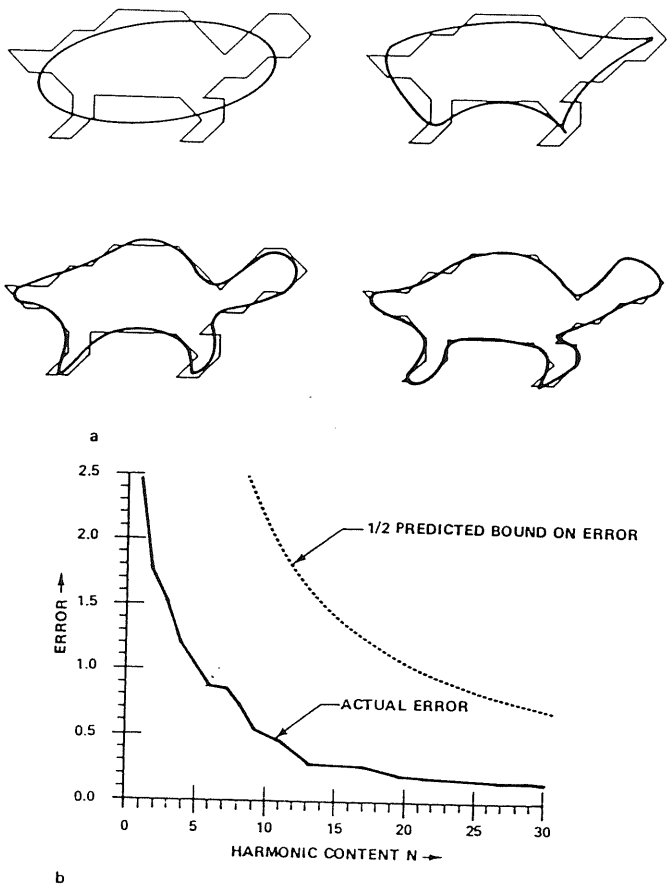

FIG. 3. Properties of the chain code V_3 = 5412343001010007711075454506541344446. (a) 1-, 4-, 8-, and 12-harmonic representations of the chain code. (b) Actual error and predicted bound on error versus harmonic content.

license for the sake of clarity, and examples of the elliptic locus of (X_1, Y_1) for a particular chain-code are given in Figs. 2 through 6. The same elliptic loci for the points (X_n, Y_n) will be obtained regardless of the starting point on the contour, but the phasors will take different orientation to approximate the contour. This will now be shown by introducing a rotational operator that relates the Fourier coefficients a_n, b_n, c_n, and d_n $(n \geq 1)$ at any starting point to the coefficients a_n^*, b_n^*, c_n^*, and d_n^* for another starting point displaced λ units around the contour, and by then comparing the loci of (X_n, Y_n) at the two starting points.

A difference in the starting points is displayed in the projected space as a phase shift; i.e., a starting point displaced λ units in the direction of rotation around the

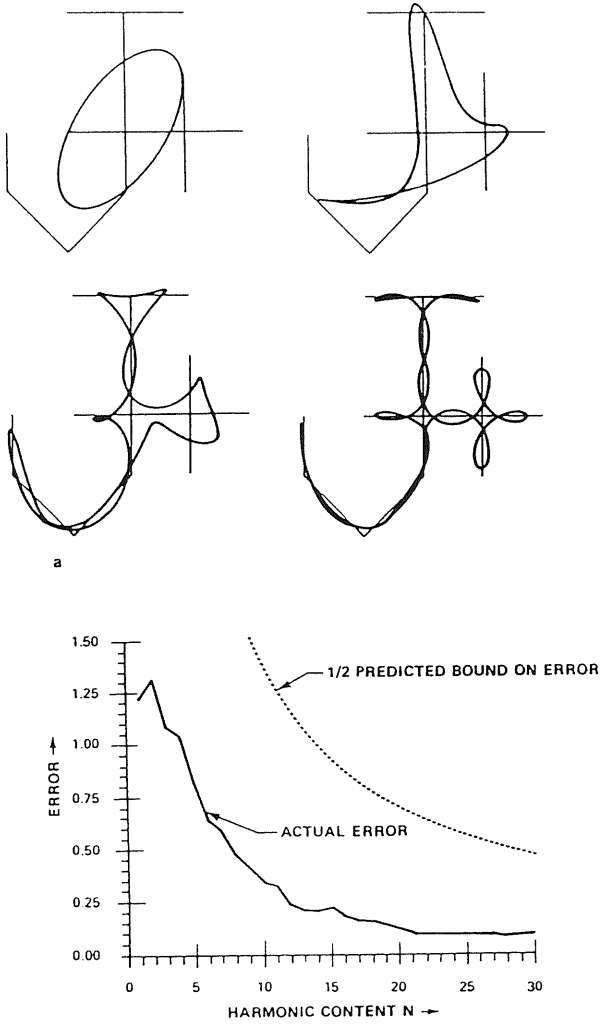

FIG. 4. Properties of the chain code V_4 = 00466026046246532671240224. (a) 1-, 3-, 7-, and 15-harmonic representations of the chain code. (b) Actual error and predicted bound on error versus harmonic content.

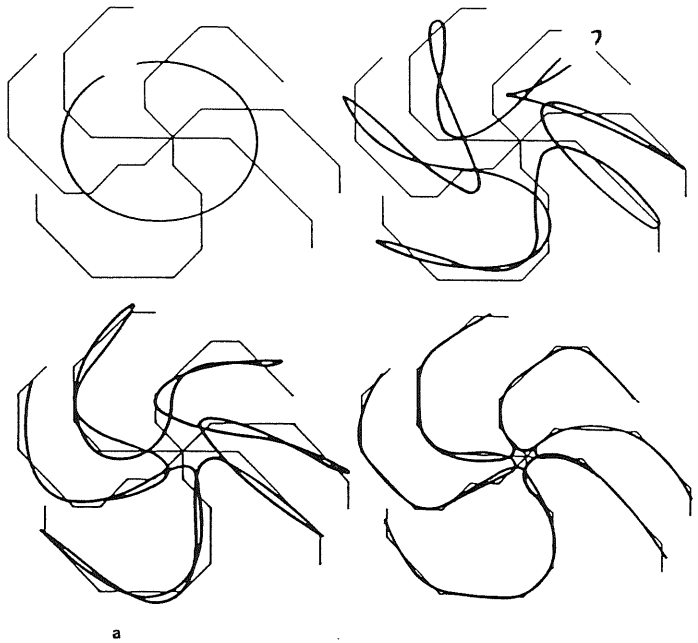

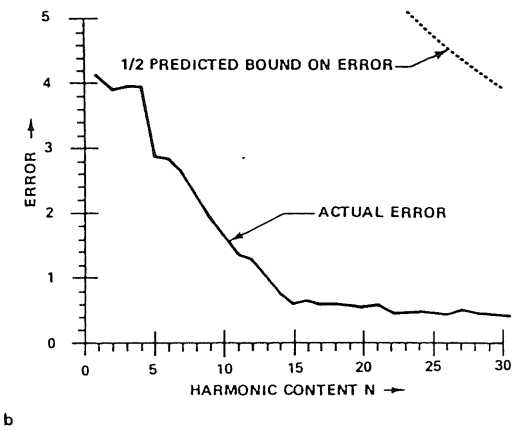

FIG. 6. Properties of the chain code V_6 = 2333446766544433267700012232545433 221566770101444322110455667000321107733455671000776233444500776. (a) 1-, 9-, 12-, and 30-harmonic representations of the chain code. (b) Actual error and predicted bound on error versus harmonic content.

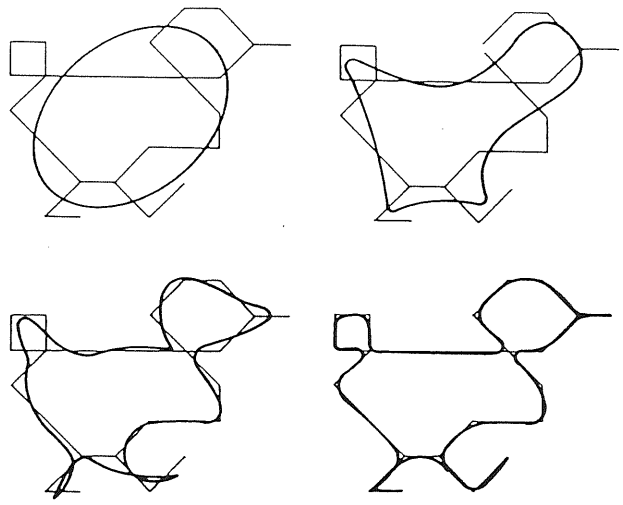

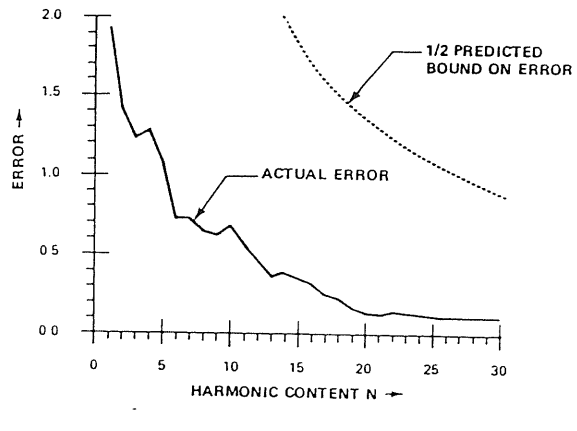

FIG. 5. Properties of the chain code V_5 = 00310704547644571534504133142060O. (a) 1-, 4-, 8-, and 12-harmonic representations of the chain code. (b) Actual error and predicted bound on error versus harmonic content.

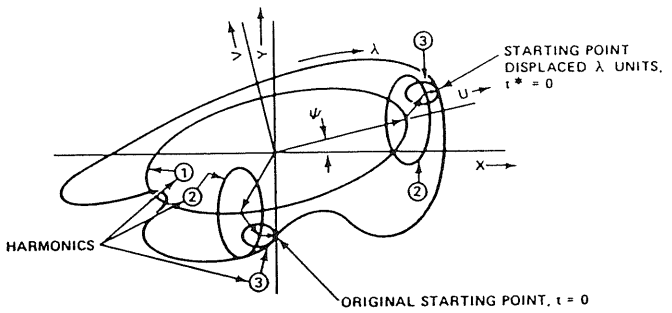

FIG. 7. Elliptic approximation to a contour.

contour from the original starting point will have projections for $n \geq 1$,

$$X_n(t^* + \lambda) = a_n \cos\frac{2\pi n}{T}(t^* + \lambda) + b_n \sin\frac{2\pi n}{T}(t^* + \lambda),$$

$$Y_n(t^* + \lambda) = c_n \cos\frac{2\pi n}{T}(t^* + \lambda) + d_n \sin\frac{2\pi n}{T}(t^* + \lambda),$$

where

$$t^* + \lambda = t.$$

Expanding X_n and Y_n and collecting terms,

$$X_n^*(t^*) = a_n^* \cos\frac{2\pi n t^*}{T} + b_n^* \sin\frac{2\pi n t^*}{T},$$

$$Y_n^*(t^*) = c_n^* \cos\frac{2\pi n t^*}{T} + d_n^* \sin\frac{2\pi n t^*}{T},$$

where

$$\begin{bmatrix} a_n^* & c_n^* \\ b_n^* & d_n^* \end{bmatrix} = \begin{bmatrix} \cos\frac{2\pi n\lambda}{T} & \sin\frac{2\pi n\lambda}{T} \\ -\sin\frac{2\pi n\lambda}{T} & \cos\frac{2\pi n\lambda}{T} \end{bmatrix} \begin{bmatrix} a_n & c_n \\ b_n & d_n \end{bmatrix}.$$

The coefficients a_n^*, b_n^*, c_n^* and d_n^* are correct for the origin of t^* (i.e., $t^* = 0$) located at the displaced starting point.

The elliptic locus for the points (X_n, Y_n) is shown by removing the dependency on the sine and cosine terms to obtain

$$\frac{(d_n^2 + c_n^2)X_n^2 + (a_n^2 + b_n^2)Y_n^2 - 2X_nY_n(a_nc_n + b_nd_n)}{(a_nd_n - b_nc_n)^2} = 1,$$

and similarly for the projections X_n^*, Y_n^*, because

$$X_n^*(t^*) = X_n(t^* + \lambda),$$

$$Y_n^*(t^*) = Y_n(t^* + \lambda),$$

$$\frac{(d_n^2 + c_n^2)X_n^{*2} + (a_n^2 + b_n^2)Y_n^{*2} - 2X_n^*Y_n^*(a_nc_n + b_nd_n)}{(a_nd_n - b_nc_n)^2} = 1.$$

Therefore, the same elliptic loci are obtained for different starting points.

Counter-clockwise rotation of the X, Y coordinate axes through ψ degrees into the U, V axes, as shown in Fig. 7, is accomplished by the rotational operation

$$\begin{bmatrix} U \\ V \end{bmatrix} = \begin{bmatrix} \cos\psi & \sin\psi \\ -\sin\psi & \cos\psi \end{bmatrix} \begin{bmatrix} X \\ Y \end{bmatrix}.$$

The effect of this axial rotation on the Fourier coefficients a_n^*, b_n^*, c_n^*, and d_n^* is readily apparent when the projections X_n^*, Y_n^* are expressed in matrix form,

$$\begin{bmatrix} X_n^* \\ Y_n^* \end{bmatrix} = \begin{bmatrix} a_n^* & b_n^* \\ c_n^* & d_n^* \end{bmatrix} \begin{bmatrix} \cos\frac{2\pi n t^*}{T} \\ \sin\frac{2\pi n t^*}{T} \end{bmatrix}.$$

Then the projections on the U, V axes u_n, v_n are

$$\begin{bmatrix} u_n \\ v_n \end{bmatrix} = \begin{bmatrix} \cos\psi & \sin\psi \\ -\sin\psi & \cos\psi \end{bmatrix} \begin{bmatrix} X_n^* \\ Y_n^* \end{bmatrix} = \begin{bmatrix} \cos\psi & \sin\psi \\ -\sin\psi & \cos\psi \end{bmatrix} \begin{bmatrix} a_n^* & b_n^* \\ c_n^* & d_n^* \end{bmatrix} \begin{bmatrix} \cos\frac{2\pi n t^*}{T} \\ \sin\frac{2\pi n t^*}{T} \end{bmatrix}$$

and an axially rotated set of Fourier coefficients a_n^{**}, b_n^{**}, c_n^{**}, and d_n^{**} may be defined as

$$\begin{bmatrix} a_n^{**} & b_n^{**} \\ c_n^{**} & d_n^{**} \end{bmatrix} = \begin{bmatrix} \cos\psi & \sin\psi \\ -\sin\psi & \cos\psi \end{bmatrix} \begin{bmatrix} a_n^* & b_n^* \\ c_n^* & d_n^* \end{bmatrix}.$$

The combined effects of an axial rotation and a displacement of the starting point on the coefficients a_n, b_n, c_n, and d_n of the original starting point are readily expressed in matrix notation as follows:

$$\begin{bmatrix} a_n^{**} & b_n^{**} \\ c_n^{**} & d_n^{**} \end{bmatrix} = \begin{bmatrix} \cos\psi & \sin\psi \\ -\sin\psi & \cos\psi \end{bmatrix} \begin{bmatrix} a_n & b_n \\ c_n & d_n \end{bmatrix} \begin{bmatrix} \cos\frac{2\pi n\lambda}{T} & -\sin\frac{2\pi n\lambda}{T} \\ \sin\frac{2\pi n\lambda}{T} & \cos\frac{2\pi n\lambda}{T} \end{bmatrix}.$$

5. ELLIPTIC FOURIER FEATURES

The Fourier coefficients a_n, b_n, c_n, and d_n $(1 \le n \le N)$ of the truncated Fourier approximation to a closed contour are used here as the classification of the contour. Since the coefficients vary according to the starting point of a trace of the contour (e.g., the Freeman chain code) and the spatial rotation, magnitude and translation of the contour, self-consistent normalization procedures based only on the intrinsic, shape properties of the contour must be specified. The rotating phasors provide the basis of a most convenient mode of normalization when the locus of the first harmonic phasor is elliptic, yielding two simply related classifications corresponding to the positions at either end of the major axis of the ellipse. When this locus is circular, useful classifications consist of the coefficient descriptions for those places on the original contour that are at a specified (e.g., maximum) distance from the contour center point (A_0, C_0). The two related methods of classification are now presented with the elliptic locus case discussed first.

5.1. *Classifications for Elliptic 1st Harmonic Locus*

A contour classification is obtained for this case in a two-step process. Initially the first harmonic phasor is rotated until it is aligned with a semi-major axis of its locus. Then the X, Y coordinate axes in which the contour was originally oriented are rotated into new U, V coordinate axes, defined by the major and minor axes of the ellipse, such that the positive X axis is coincident with the semimajor axis located in the phasor rotation. The existence of only two possible classifications is easily verified by constructing phasor-addition diagrams of contours similar to those shown in Fig. 7 for different combinations of rotations and by observing that the phasor additions at each semimajor axis are always oriented the same way in the framework of the U, V coordinate axes. To determine the relationship between the two classifications, let the classification associated with one semimajor axis be obtained through starting-point and spatial angular rotations of θ_1 and ψ_1 radians, respectively, where $\theta_1 = 2\pi\lambda_1/T$ and λ_1 is the displacement of the starting point. Then the classification for the semimajor axis is $(1 \le n \le N)$

$$\begin{bmatrix} {}_1a_n^{**} & {}_1b_n^{**} \\ {}_1c_n^{**} & {}_1d_n^{**} \end{bmatrix} = \begin{bmatrix} \cos\psi_1 & \sin\psi_1 \\ -\sin\psi_1 & \cos\psi_1 \end{bmatrix} \begin{bmatrix} a_n & b_n \\ c_n & d_n \end{bmatrix} \begin{bmatrix} \cos n\theta_1 & -\sin n\theta_1 \\ \sin n\theta_1 & \cos n\theta_1 \end{bmatrix}.$$

The classification for the other semimajor axis is obtained by a further rotation of both the starting-point and spatial angles through π radians as follows:

$$\begin{aligned} \begin{bmatrix} {}_2a_n^{**} & {}_2b_n^{**} \\ {}_2c_n^{**} & {}_2d_n^{**} \end{bmatrix} &= \begin{bmatrix} \cos(\psi_1+\pi) & \sin(\psi_1+\pi) \\ -\sin(\psi_1+\pi) & \cos(\psi_1+\pi) \end{bmatrix} \begin{bmatrix} a_n & b_n \\ c_n & d_n \end{bmatrix} \\ &\quad \times \begin{bmatrix} \cos n(\theta_1+\pi) & -\sin n(\theta_1+\pi) \\ \sin n(\theta_1+\pi) & \cos n(\theta_1+\pi) \end{bmatrix} \\ &= -\begin{bmatrix} \cos\psi_1 & \sin\psi_1 \\ -\sin\psi_1 & \cos\psi_1 \end{bmatrix} \begin{bmatrix} a_n & b_n \\ c_n & d_n \end{bmatrix} (-1)^n \begin{bmatrix} \cos n\theta_1 & -\sin n\theta_1 \\ \sin n\theta_1 & \cos n\theta_1 \end{bmatrix} \\ &= (-1)^{n+1} \begin{bmatrix} {}_1a_n^{**} & {}_1b_n^{**} \\ {}_1c_n^{**} & {}_1d_n^{**} \end{bmatrix}. \end{aligned}$$

Therefore, the odd harmonics of the two classifications remain the same for all n, but the even harmonics (not including the bias terms A_0 and C_0) change sign.

The starting-point, angular rotation θ_1, is determined from the point (x_1, y_1) with elliptic locus

$$\begin{aligned} x_1 &= a_1\cos\theta + b_1\sin\theta, \\ y_1 &= c_1\cos\theta + d_1\sin\theta, \end{aligned}$$

where $\theta = 2\pi t/T$, by differentiating the magnitude of the first harmonic phasor $E = (x_1^2 + y_1^2)^{1/2}$ and setting the derivative equal to zero, which yields

$$\theta_1 = \frac{1}{2}\arctan\left[\frac{2(a_1b_1 + c_1d_1)}{a_1^2 + c_1^2 - b_1^2 - d_1^2}\right].$$

This expression locates the first semimajor axis to occur moving away from the starting point in the direction of rotation about the contour. This can be proven by substituting the value of θ_1 in the second derivative of E and noting that a negative quantity is always obtained; i.e., $0 \le \theta_1 < \pi$.

The spatial rotation ψ_1 is determined from the Fourier coefficients a_1^* and c_1^* that are correct for the starting point displaced θ_1 radians. Now

$$\begin{bmatrix} a_1^* & c_1^* \\ b_1^* & d_1^* \end{bmatrix} = \begin{bmatrix} \cos\theta_1 & \sin\theta_1 \\ -\sin\theta_1 & \cos\theta_1 \end{bmatrix} \begin{bmatrix} a_1 & c_1 \\ b_1 & d_1 \end{bmatrix}$$

and the point (x_1^*, y_1^*) with elliptic locus is

$$\begin{aligned} x_1^*(t^*) &= a_1^*\cos\frac{2\pi}{T}t^* + b_1^*\sin\frac{2\pi}{T}t^*, \\ y_1^*(t^*) &= c_1^*\cos\frac{2\pi}{T}t^* + d_1^*\sin\frac{2\pi}{T}t^*. \end{aligned}$$

Since $t^* = 0$ when the first harmonic phasor is aligned with the semimajor axis, ψ_1 is readily obtained as

$$\begin{aligned} \psi_1 &= \arctan\left[\frac{y_1^*(0)}{x_1^*(0)}\right] \\ &= \arctan\frac{c_1^*}{a_1^*}, \quad 0 \le \psi_1 < 2\pi. \end{aligned}$$

Furthermore, the magnitude of the semimajor axis is

$$\begin{aligned} E^*(0) &= \left(x_1^*(0)^2 + y_1^*(0)^2\right)^{1/2} \\ &= \left(a_1^{*2} + c_1^{*2}\right)^{1/2}. \end{aligned}$$

The classification can be made independent of size by dividing each of the coefficients by the magnitude of the semimajor axis, and independent of translation by

ignoring the bias terms A_0 and C_0. It should be noted that the first harmonic content of the size-normalized classification is always characterized by $a_1^{**} = 1.0$, $b_1^{**} = 0.0$, $c_1^{**} = 0.0$, and $|d_1^{**}| < 1.0$.

An example of the elliptic classification procedure is shown for the tank on an incline in Fig. 8. In Fig. 8a the image and the first harmonic ellipse are shown and in Fig. 8b the 30th harmonic approximation of the tank is given. In Fig. 8c the two possible classifications involving the 30th harmonic approximation are shown by solid and dotted lines, respectively, as generated by the normalized coefficients.

5.2. *Classifications for Circular 1st Harmonic Locus*

A contour classification for this case is obtained in a manner analogous to the elliptical case except that the starting-point and spatial rotations cannot be made to a semimajor axis. Instead, the rotations are made to the line emanating from the bias point (A_0, C_0) to the point on the contour most distant from the bias point. If several such maximal points on the contour are equidistant from (A_0, C_0) then a like

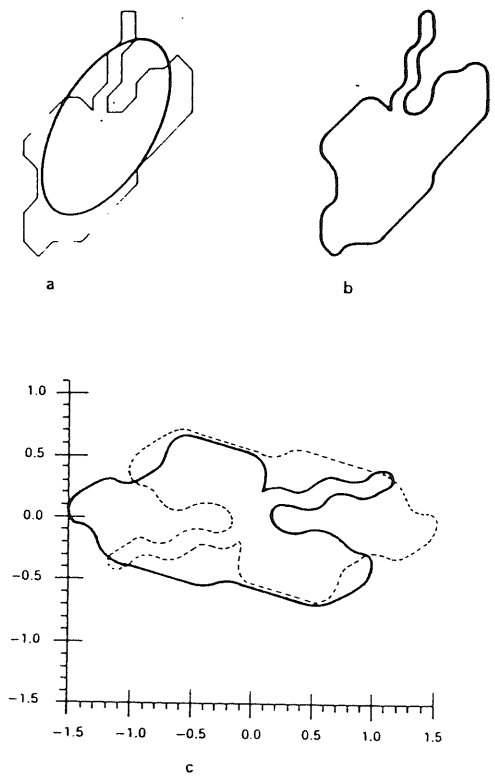

FIG. 8. A tank and its two possible classifications. (a) A tank and its 1st harmonic ellipse. (b) The 30th harmonic representation of the tank. (c) The two possible classifications of the tank.

number of classifications will be obtained. Working with the previously described chain code representation of the contour the candidate distances E_p $(1 \le p \le K)$ will be among the bias point (A_0, C_0) and the heads of the chain links a_p. Each distance E_p is

$$E_p = \left((A_0 - x_p)^2 + (C_0 - y_p)^2\right)^{1/2}.$$

The indices of p corresponding to equally large maxima are stored and a classification is required for each one. The starting-point rotation θ_p for a classification corresponding to index p is

$$\theta_p = \frac{2\pi t_p}{T}, \qquad 0 < \theta_p \le 2\pi,$$

and the spatial rotation angle ψ_p is

$$\psi_p = \arctan\left[\frac{y_p - C_0}{x_p - A_0}\right], \qquad 0 \le \psi_p < 2\pi.$$

The classification for index p is then

$$\begin{bmatrix} {}_pa_n^{**} & {}_pb_n^{**} \\ {}_pc_n^{**} & {}_pd_n^{**} \end{bmatrix} = \begin{bmatrix} \cos\psi_p & \sin\psi_p \\ -\sin\psi_p & \cos\psi_p \end{bmatrix} \begin{bmatrix} a_n & b_n \\ c_n & d_n \end{bmatrix} \begin{bmatrix} \cos n\theta_p & -\sin n\theta_p \\ \sin n\theta_p & \cos n\theta_p \end{bmatrix}.$$

Size normalization of the classification is again accomplished by dividing each of the Fourier coefficients by $[a_1^2 + c_1^2]^{1/2}$, which is the radius of the first harmonic circle. Note, the first harmonic locus is a circle when

$$a_1^2 + b_1^2 + c_1^2 + d_1^2 = 2(a_1 d_1 - b_1 c_1).$$

If a contour can be rotated by $360°/m$ (where m is an integer ≥ 3) so as to coincide with itself, it will have a circular first harmonic locus and only one unique classification. Examples of such contours are squares and pentagons, and hurricane-like figures with many identical, equispaced, swirling, S-shaped arms. An example of the classification procedure for a windmill blade is shown in Fig. 9. In Figs. 9a and b, the blade, the first harmonic circle, and the thirteenth harmonic approximation of the blade are given. In Fig. 9c, the classification involving the first thirteen harmonics is shown as generated from the normalized coefficients.

The circle-case normalization procedure can be modified to act as a substitute for the elliptic-case procedure by employing a different method of size normalization; i.e., by normalizing the magnitude of the coefficients against the maximal distance E_p.

6. RECOGNITION DECISIONS

The contour classifications are used in both a training (i.e., library cataloging) mode for known examples of classes and a decision mode for recognizing unknown images. The rotation and size normalized classifications stored for a known class m

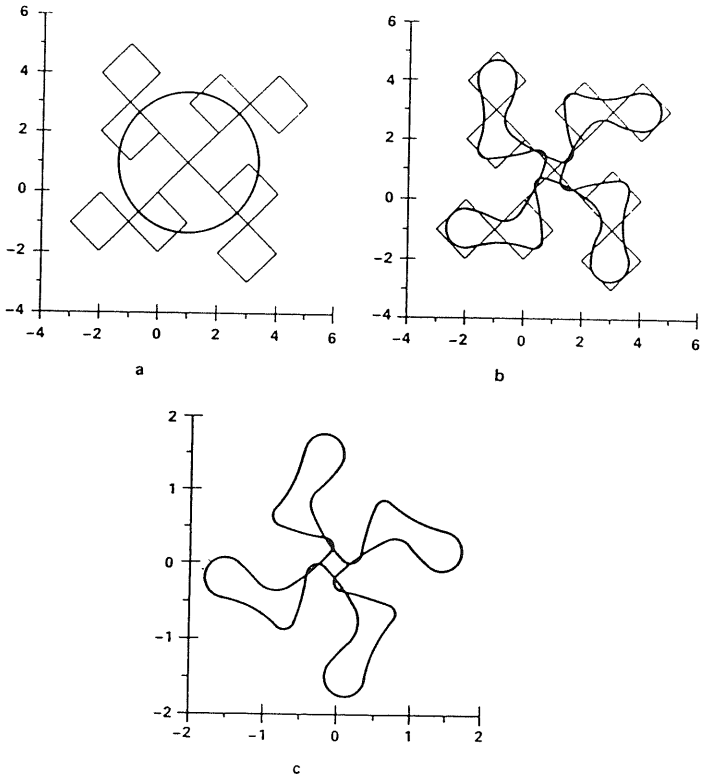

FIG. 9. Example of circle-case approximation. (a) Windmill blade and 1st harmonic approximation. (b) Windmill blade and 13th harmonic approximation. (c) Normalized 13th harmonic approximation of windmill blade.

are

$$\begin{bmatrix} {}_pa_{nm}^{**} & {}_pb_{nm}^{**} \\ {}_pc_{nm}^{**} & {}_pd_{nm}^{**} \end{bmatrix}.$$

Translation is ignored by omitting the bias coefficients. For the case of an elliptic first harmonic locus the classification indices corresponding to the two semi-major axes are $p = 1, 2$ and for the case of a circular first harmonic locus with P equidistant maximal contour points, $p = 1, 2, \ldots, P$. The normalized classifications for an unknown image are

$$\begin{bmatrix} {}_ra_n^{**} & {}_rb_n^{**} \\ {}_rc_n^{**} & {}_rd_n^{**} \end{bmatrix},$$

where the classification index r is defined identically to that of p for a known class.

A metric distance, D_m, between the known class m and the unknown image is defined as the combined minimum over the classification indices r and p.

$$D_m^2 = \min_{r=1,2,\ldots,R}\left[\min_{p=1,2,\ldots,P}\sum_{n=1}^{N} D_n^2(r, p, m)\right],$$

where

$$D_n^2(r, p, m) = \left({}_ra_n^{**} - {}_pa_{nm}^{**}\right)^2 + \left({}_rb_n^{**} - {}_pb_{nm}^{**}\right)^2 + \left({}_rc_n^{**} - {}_pc_{nm}^{**}\right)^2 + \left({}_rd_n^{**} - {}_pd_{nm}^{**}\right)^2.$$

The expression for D_m reduces according to the number of values of p that are stored for class m and the number of values of r computed for the unknown image. For example, if only one value of r is computed for the unknown image the expression reduces to a minimum over the p index. And, if all values of r are computed for the unknown image but only one value of p is stored the expression reduces to a minimum over the r index. The minimum of the distances D_m $(1 \le m \le M)$, among the unknown image and the known classes determines the class of the unknown image.

It is clear that in dealing with continuous, unquantized contours the Fourier descriptors will give unique, separable classifications as long as enough harmonics are included in the truncated Fourier series, and that the Fourier descriptors are therefore good for template matching applications. However, in sampling these contours some information is destroyed according to the coarseness of the sampling interval and the contours will, in general, be encoded differently for each particular orientation on the sampling grid. The result is a nonzero metric, D, among the normalized classifications of the same contour for different relative grid orientations and grid coarsenesses. The importance of these effects is of course extremely dependent on the application and the inherent separability of the classes of interest, and merits a case-by-case statistical examination in arriving at an overall system design. A simple example of the quantization effect on the metric is given for the airplane images in Fig. 10, each of which is derived from the same original unquantized image. The image shown at the top left of the figure has the highest resolution and consists of pixels of unit size on edge while the other images have progressively lower resolution and consist of respective pixel sizes of 2, 3, 4, and 5 units on edge, which are indicated in Roman numerals. Normalized image classifications at each level of resolution are shown for harmonic truncations $N = 7$, 14, 21, and 28. The metric matrices for harmonic truncations of $N = 7$, 14, 21, and 28 are shown in Table 2, and each matrix corresponds to its respective row N of normalized classifications in Fig. 10. It is noted that the metric among different grid resolutions becomes greater as the harmonic content increases, as expected from inspection of the expression for D. What is surprising is that the metric among different resolutions does not necessarily increase as the separation among the resolutions increases. This experimental result is an indication that the Fourier-coefficient classifications will tend to cluster in the classification space for different pixel resolutions across an image.

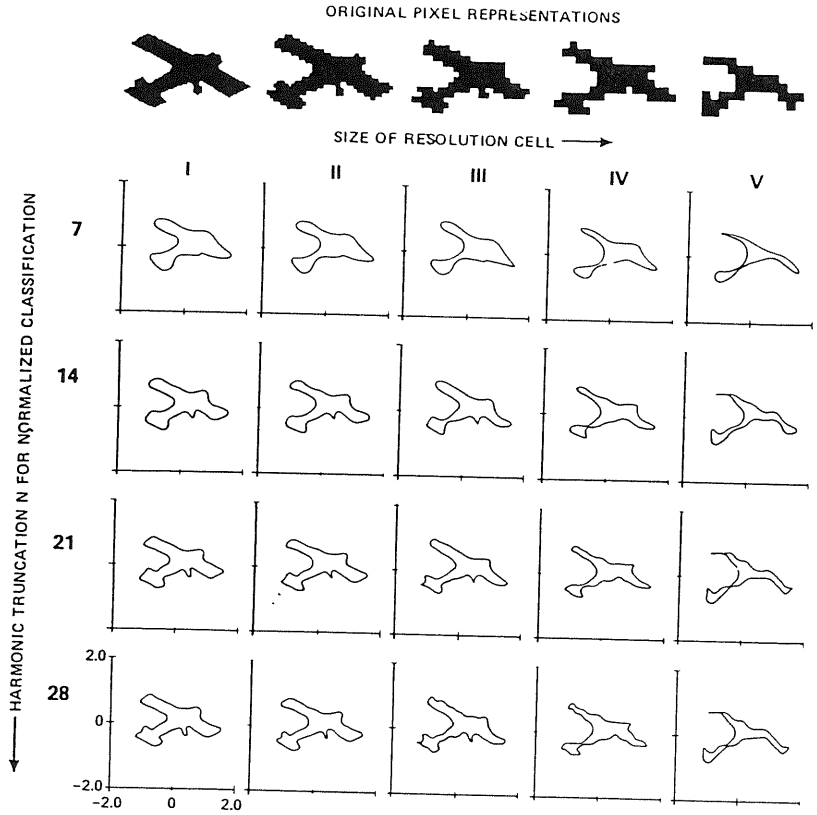

FIG. 10. Example of quantization effect on image normalization.

7. RECOGNITION OF SOLID OBJECTS AT ARBITRARY ASPECT ANGLE

A recognition system for arbitrarily shaped, solid objects at arbitrary aspect angle that uses elliptic Fourier features is proposed here as an extension of the image recognition system already discussed. The system requires that detailed a priori knowledge be available about the shape of the object. The system assumes that aspect can be resolved into three components—roll, pitch, and yaw—and that the coordinate axes are located at the center of gravity of the object, with one axis in the observer's line of sight about which pitch changes.

The elliptic Fourier feature set is invariant with pitch, but for arbitrary bodies the variation as a function of yaw and roll is quite complicated. Therefore, the feature set must be represented in a $4 \times N$ classification space as a toroidal surface, which can be approximated by a single closed line that itself consists of closed curves and connecting line segments. Each closed curve traces the feature set variation with 360° of roll for a particular yaw angle, and each connecting line segment traces the feature set variation with an incremental change of the yaw angle for a constant roll angle. The classification surface contour is traced out, starting at 0° roll and yaw, by following these roll and yaw curves in proper sequence and without repetition so that all are included.

Recognition of an unknown body requires a means of measuring the mean square distances between multiple observations of it and the classification surfaces of known body shapes. A procedure for encoding such surfaces and performing recognition decisions using n-dimensional chain codes is discussed by Kuhl [10] and Kuhl and Perrella [11] in relation to the recognition of arbitrary targets at arbitrary aspect angle using polarized radar-backscatter measurements.

TABLE 2

Metric Matrices for the Five Different Resolution Images in Fig. 10 at Harmonic Truncations of $N = 7, 14, 21$, and 28

			Resolution cell size				
			1	2	3	4	5
Harmonic truncation = 7	Resolution cell size	1	0.000000	.057901	.209273	.216583	.318336
		2	.057901	0.000000	.177079	.176443	.272942
		3	.209273	.177079	0.000000	.248555	.287131
		4	.216583	.176443	.248555	0.000000	.194504
		5	.318336	.272942	.287131	.194504	0.000000

			Resolution cell size				
			1	2	3	4	5
Harmonic truncation = 14	Resolution cell size	1	0.000000	.066026	.219366	.239670	.337399
		2	.066026	0.000000	.185995	.199620	.294752
		3	.219366	.185995	0.000000	.262008	.300132
		4	.239670	.199620	.262008	0.000000	.214473
		5	.337399	.294752	.300132	.214473	0.000000

			Resolution cell size				
			1	2	3	4	5
Harmonic truncation = 21	Resolution cell size	1	0.000000	.070559	.222526	.244808	.338798
		2	.070559	0.000000	.188583	.205077	.296366
		3	.222526	.188583	0.000000	.265366	.301661
		4	.244808	.205077	.265366	0.000000	.218607
		5	.338798	.296366	.301661	.218607	0.000000

			Resolution cell size				
			1	2	3	4	5
Harmonic truncation = 28	Resolution cell size	1	0.000000	.072647	.223299	.246054	.339471
		2	.072647	0.000000	.189842	.206575	.296969
		3	.223299	.189842	0.000000	.267048	.302408
		4	.246054	.206575	.267048	0.000000	.219584
		5	.339471	.296969	.302408	.219584	0.000000

8. CONCLUSION

A classification and recognition procedure has been described that is dire applicable to classes of objects that cannot change shape and whose images are subject to sensory-equipment distortions, but that may occur in different orie tions, sizes and translations. The features used in the procedure are normali Fourier coefficients derived from chain codes of the image contours. The normal tion is performed according to various elliptic properties of the Fourier coeffici themselves.

ACKNOWLEDGMENTS

The authors wish to express their appreciation for a well done computer progra ming effort to Dorothy Heater, Mary Jane Webster, and Michael Kajor. Heart thanks are also due to Maxine Barrett Kuhl for her considerable efforts in edit this paper.

REFERENCES

1. G. H. Granlund, Fourier preprocessing for hand print character recognition, *IEEE Trans. Com* **C-21**, 1972, 195–201.
2. E. Persoon and K. S. Fu, Shape discrimination using Fourier descriptors, *IEEE Trans. Systems, M Cybernetics* SMC-7, 1977, 170–179.
3. T. P. Wallace and P. A. Wintz, An efficient three-dimensional aircraft recognition algorithm us normalized Fourier descriptors, *Computer Graphics and Image Processing* **13**, 1980, 99–126.
4. T. P. Wallace and O. R. Mitchell, Analysis of three-dimensional movement using Fourier descript *IEEE Trans. Pattern Analysis and Machine Intelligence* **PAMI-2**, 1980, 583–588.
5. H. Freeman, Computer processing of line drawing images, *Comput. Surv.* **6**, 1974, 57–97.
6. F. Kuhl, Criteria for determining contour resolution using harmonically related ellipses, Proceed of the IEEE Region 3 Convention (Southeast Con), University of Tennessee, Knoxville, Ten see, April 10–12, 1972, pp. S-5-1, S-5-4.
7. C. Giardina and F. Kuhl, Accuracy of curve approximation by harmonically related vectors w elliptical loci, *Computer Graphics and Image Processing* 6, 1977, 277–285.
8. F. P. Kuhl, Classification and recognition of hand-printed characters, IEEE International Convent Record, Pt. 4, 1963, pp. 75–93.
9. H. Freeman, Application of the generalized chain coding scheme to map data processing, Proceedi of the IEEE Computer Society Conference on Pattern Recognition and Image Process Chicago, Illinois, May 31–June 2, 1978.
10. F. P. Kuhl, Recognition of geometric classes in free space, Proceedings of the IEEE Regi Convention (Southeast Con), University of Louisville, Louisville, Kentucky, April 30–M 1973, pp. F-5-1, F-5-4.
11. F. P. Kuhl and A. J. Perrella, Radar target recognition at arbitrary aspect, Proceedings of the IE Region 3 Convention (Southeast Con), University of Virginia, Charlottesville, Virginia, A 26–28, 1971, pp. 411–416.
12. F. P. Kuhl, C. R. Giardina, M. J. Webster and D. O'Connor, Fourier series approximation chain-encoded contours, Proceedings of the Electro-Optics/Laser 80 Conference & Exposit Boston, Massachusetts, November 19–21, 1980.